



# Adhesion/atomistic friction surface interaction model with application to interfacial fracture and nanofabrication

E.D. Reedy Jr. \*

Sandia National Laboratories, Albuquerque, NM 87185, USA

## ARTICLE INFO

### Article history:

Received 11 May 2012

Received in revised form 19 November 2012

Available online 14 December 2012

### Keywords:

Interfacial fracture  
Adhesion

## ABSTRACT

A novel adhesion/atomistic friction (Ad/AF) surface interaction model has been developed for solid materials interacting through van der Waals dispersive forces. This model was motivated by friction force microscopy data that suggest that in at least some cases a pressure-independent interfacial shear strength can be used to describe molecular-level friction. The Ad/AF model has two elements. Adhesion is defined by a traction–separation relationship, where the key parameters are interfacial strength and the work of adhesion. The second element of the Ad/AF model defines the nature of interfacial shear stress in a way that is consistent with a pressure-independent interfacial shear strength. The model assumes friction acts only when the opposing materials are in contact. The Ad/AF model, which has been implemented within an explicit dynamics finite element code, has been applied to several problems where adhesion and atomistic friction are expected to play an important role. Illustrative results from interfacial fracture and nano-embossing simulations are presented. The fracture simulation shows that the Ad/AF surface interaction model generates a strongly mode-dependent effective interfacial toughness (i.e., depends on the relative level of the applied shear). The nano-embossing simulations indicate that even low levels of adhesion and atomistic friction can have a significant effect on nanofabrication processes.

© 2012 Published by Elsevier Ltd.

## 1. Introduction

Adhesion and atomistic friction can have a major impact on the operation and performance of a variety of technologically important devices. Here the focus is on solids that interact through van der Waals forces. Although such forces are relatively weak compared to those generated by chemical bonds, they can still generate significant deformations when an object is sufficiently compliant. One well-known example that clearly demonstrates the necessity of taking adhesion into account is the observed deformation of contacting rubbery spheres. The Johnson–Kendall–Roberts (JKR) contact mechanics analysis was developed over 40 years ago to explain how adhesion can markedly increase the contact radius between smooth rubbery spheres relative to that which would occur if Hertz contact theory applied (Johnson et al., 1971). Furthermore, unlike the Hertz contact theory, the JKR analysis predicts the observed tensile pull-off load. The adhesion-dependent contact of soft materials is a topic of continuing interest. For example, in recent years ways of mimicking bio-inspired adhesion via micrometer-scale patterned soft materials has received considerable

attention (Glassmaker et al., 2004; Crosby et al., 2005). Typically the goal of this work is to enhance the adhesion between materials relative to that attainable with flat surfaces. Adhesion effects can also be significant in devices that are fabricated from a relatively high modulus material when the length-scale of the device decreases. For example, microelectromechanical systems (MEMS) devices fabricated using surface micromachining techniques can contain exceedingly compliant polycrystalline silicon beams. The deflection of such beams can be altered by adhesion (DelRio et al., 2005). Adhesion can even cause MEMS devices to fail when a shock loading causes unintentional adhesive contact that cannot be broken by the elastic restoring forces (Maboudian et al., 2002). Adhesion effects can also have a substantial impact on micro/nano-fabrication processes. Adhesion can cause the pattern in the elastomer stamp used in microcontact printing to collapse when feature aspect ratios exceed stability limits (Hui et al., 2002). In nanoimprint lithography, the adhesion between a stiff mold and the polymer imprint must be made sufficiently weak to enable a clean separation during release so as to minimize the formation of defects in the pattern (Gates et al., 2005; Costner et al., 2009). These examples suggest the sort of interesting problems that can be analyzed when a suitable adhesive surface interaction model is implemented in a finite element analysis code. Also note that atomistic friction can generate large tangential tractions on adhered, sliding

\* Tel.: +1 5058443297.

E-mail address: [edreedy@sandia.gov](mailto:edreedy@sandia.gov)

surfaces. Such forces can exist, for example, in MEMS devices that allow contact between surfaces (Corwin and de Boer, 2004), or between surfaces that are peeled apart (Newby et al., 1998). The inclusion of atomistic friction in the surface interaction model enables nano-scale simulations of problems where interfacial slip occurs.

The adhesion/atomistic friction (Ad/AF) surface interaction model used in this study was motivated by friction force microscopy measurements. In these scanning probe tests of solids that interact through van der Waals dispersive forces, the friction (lateral) force that opposes slip is measured as a function of the applied normal force. Published work suggests that in at least some circumstances, a pressure-independent interfacial shear strength can be used to describe atomic-scale frictional slip in such tests (Burns et al., 1999; Carpick et al., 2004). Specifically,

$$F = \tau^* A \quad (1)$$

where  $F$  is friction force,  $\tau^*$  is a constant interfacial shear strength, and  $A$  is the contact area that depends on both adhesion and the applied normal load. Note that the work of adhesion can be determined from the pull-off load (Johnson et al., 1971; Derjaguin et al., 1975; Reedy, 2007). Data measured in several friction force microscopy studies of polymer coatings on hard substrates have been found to be consistent with Eq. (1). This includes friction data for a glass tip interacting with model lubricant silane and alkanethiol self-assembled monolayers (Burns et al., 1999), a silicon atomic force microscope (AFM) tip sliding over an OTS (octadecyltrichlorosilane) self-assembled monolayer-coated silicon substrate (Reedy et al., 2005), and an AFM tip coated with a variety of self-assembled aromatic compounds sliding along a similarly coated substrate (Yang and Ruths, 2009). These results suggest that the friction response defined by Eq. (1) is generally applicable to thin nanometer-scale polymer coatings. Such coatings can be formulated to perform as anti-adhesion coatings. It is also possible that Eq. (1) is generally applicable to polymer/solid interactions even when the adjacent materials are not thin coatings since atomistic friction is a surface property.

## 2. Adhesion/atomistic friction surface interaction model

The adhesion/atomistic friction (Ad/AF) surface interaction model is based on atomistic frictional behavior as described by Eq. (1). This model has two elements. Adhesion is defined by a traction–separation ( $T$ – $U$ ) relationship, where  $\sigma$  is the normal traction and  $\delta_n$  is the normal interfacial separation (Fig. 1a). This relationship holds when  $\delta_n \geq 0$ , otherwise normal interpenetration is prevented (e.g., by a finite element analysis's contact algorithm). The two key parameters defining this  $T$ – $U$  relationship are the interfacial strength  $\sigma^*$  and the work of adhesion  $\Gamma$ . This study uses a

simple triangular  $T$ – $U$  relationship with a steep initial portion (defined by  $\lambda$ , with a typical value of 0.05, see Fig. 1a) and a finite cut-off distance for the adhesive force  $\delta_n^c$ . For a triangular  $T$ – $U$  relationship, the work of adhesion  $\Gamma$ , which equals the area under the  $T$ – $U$  curve, has a value of  $\sigma^* \delta_n^c / 2$ . Materials interact via the  $T$ – $U$  relationship whenever they are within a distance  $\delta_n^c$  of each other whether approaching or separating. One can make a rough estimate for the model parameters used in the adhesion model. The work of adhesion for a polymer/solid interface can be relatively low when the solids interact only via van der Waals forces (i.e., no chemical bonding). For example,  $\Gamma$  for an epoxy/OTS interface has been measured to be  $\sim 0.05 \text{ J/m}^2$  (Kent et al., 2001). Furthermore, the bulk of the work done to separate materials that interact via van der Waals forces occurs while the materials are within  $\sim 1 \text{ nm}$  (Kendall, 1994). Accordingly, when  $\Gamma = 0.05 \text{ J/m}^2$ , the interfacial strength  $\sigma^*$  equals 100 (50) MPa when  $\delta_n^c$  equals 1 (2) nm (assuming a triangular  $T$ – $U$  relationship). Since the  $T$ – $U$  relationship includes a length scale, calculated results are mesh-independent provided that the mesh is fine enough to resolve the open gap across which adhesive forces act. The adhesion portion of the Ad/AF model is a simple, Mode I only version of what is now commonly referred to as a cohesive zone model (Barrenblatt, 1962; Needleman, 1987; Tvergaard and Hutchinson, 1992). Note, however, here the model applies not only to separating initially bonded materials but also when materials jump into contact.

The second element of the Ad/AF model defines the nature of interfacial shear stress  $\tau$  in a way that is consistent with Eq. (1) (Fig. 1b). Here it is assumed that there is no frictional interaction between opposing materials when  $\delta_n > \lambda \delta_n^c$ . In this study  $\lambda$  was set equal to 0.05 and consequently  $\lambda \delta_n^c$  equals 0.05 nm when  $\delta_n^c = 1 \text{ nm}$ . This value of  $\lambda \delta_n^c$  is comparable to atomistic roughness (the surface is assumed to be otherwise smooth on a length scale commensurate with the range of the adhesive force,  $\delta_n^c$ ). Friction does not act across an open gap with  $\delta_n > \lambda \delta_n^c$ , and consequently  $\tau = 0$  when this condition applies. Friction acts only when  $\delta_n < \lambda \delta_n^c$ . When friction acts, the opposing materials are tied together if  $|\tau| < \tau^*$ , while slip occurs when  $|\tau| = \tau^*$ , with  $\tau^*$  opposing frictional slip  $\delta_t$  (note,  $\tau^*$  is a pressure-independent material constant). One virtue of the Ad/AF model is that the most important of the parameters defining the model ( $\Gamma$  and  $\tau^*$ ) can be deduced from friction force microscopy measurements.

The analysis was performed using Sandia National Laboratories' Sierra/SM explicit, transient dynamics finite element code (Thomas, 2011). In brief, an explicit dynamics finite element analysis uses a central difference time integrator to advance the solution from an initial state using time steps that satisfy a stability criterion. Explicit dynamics finite element codes are well suited for analyzing large deformations with complex contact conditions, discontinuous crack growth, etc. The Ad/AF model is implemented

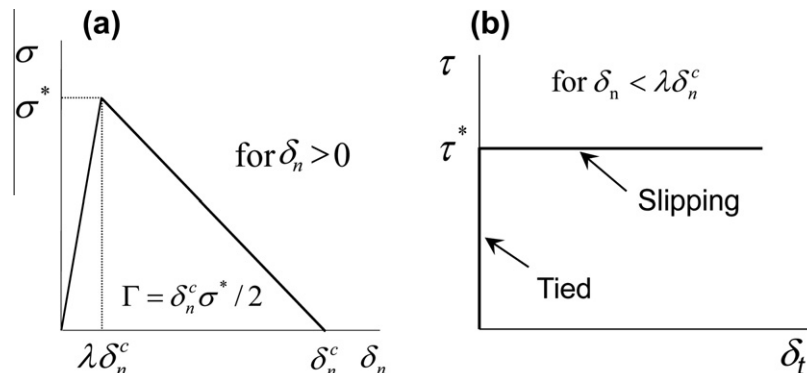


Fig. 1. (a) adhesion and (b) atomistic friction portions of Ad/AF surface interaction model, where  $\tau^*$  opposes frictional slip  $\delta_t$ .

in the Sierra/SM explicit finite element code via an extension of its contact algorithm. As implemented, the Ad/AF finite element analysis implicitly assumes that the interface is locally flat on a length scale commensurate with the range of the adhesive force (e.g., model geometry does not contain features with size  $< \delta_n^c$ ). Note that adhesive forces are calculated in the current, deformed geometry with gap distance defined by the normal distance between a node and the opposing surface. Thus, opposing materials can undergo large relative translations and still interact if they are within the range of the adhesive force. For example, the Ad/AF model allows separation and reattachment after a large relative tangential displacement. To model such large displacement phenomena, a contact algorithm-based implementation of the Ad/AF model is preferred to one based upon interface elements. In all calculations reported here, the external loads are applied sufficiently slowly that the external loading is quasistatic. Nevertheless, an interfacial separation can still propagate dynamically once initiated if the energy release rate exceeds the interfacial resistance to separation. As reported previously, the accuracy of the adhesion portion of the Ad/AF model has been verified by simulating a problem where the JKR adhesion analysis should apply (Reedy, 2006). In the following, illustrative results demonstrating the use of the Ad/AF surface interaction model are presented. The model is first applied to a classical interfacial fracture problem where two solid materials that are initially in contact are pulled apart and then to an idealized nano-embossing problem where two materials that are initially separated are brought into contact.

### 3. Interfacial fracture

The impact of using the Ad/AF surface interaction model in an interfacial fracture analysis is illustrated by analyzing the classic problem of bimaterial strip with a long edge crack held between rigid grips (Fig. 2). In a further simplification of this plane strain analysis, the upper material is treated as rigid while the lower material is linear elastic (with Young's modulus  $E$ , Poisson's ratio  $\nu$ , and density  $\rho$ ). The dimensions of the strip model used in the finite element analysis were chosen so as to closely approximate an infinitely long strip with a semi-infinite interfacial crack. The height  $h$  of the elastic layer is equal to  $1 \mu\text{m}$ , while the crack length  $a$  equals  $6 \mu\text{m}$  and the strip length  $L$  equals  $18 \mu\text{m}$ . The strip is loaded by applying uniform edge-normal and edge-tangential displacements to the upper rigid material while the bottom edge of the lower elastic material is fixed. Test calculations showed that the strip is sufficiently long so as to generate a large uniformly stressed region in the central portion of the ligament with stress levels equal to those in an infinitely long strip. The applied edge velocity of  $0.1 \mu\text{m}/\mu\text{s}$  is slow enough that inertial effects due to the applied loading are negligible. The finite element model geometry has a highly refined mesh in a  $2h/5$  wide by  $h/5$  high region that surrounds the initial crack tip. In this region, the characteristic element size  $\Delta$  equals  $0.0025 \mu\text{m}$  ( $h/400$ ). A low level of mass damping (as specified by a Rayleigh mass damping coefficient  $m_d$ ) is used in these explicit dynamics finite element calculations to damp out vibrations (stress waves) generated by the release of interfacial shear stress as the adhesive zone forms. Mass

proportional damping is simply a convenient way to include damping in the calculations.

The interface's effective toughness  $\Gamma_e$  is defined as the value of the energy release rate when the interfacial crack begins to propagate. This is calculated using the well-known analytical energy release rate calibration for an edge-cracked bimaterial strip held between rigid grips where one material is rigid

$$\Gamma_e = \frac{h}{2E_u} (\sigma_{yy}^c)^2 + \frac{h}{2G} (\sigma_{xy}^c)^2 \quad (2)$$

and where  $\sigma_{yy}^c$  and  $\sigma_{xy}^c$  are the calculated critical values of the normal and shear stress in the uniformly stressed ligament when the crack begins to propagate,  $E_u = (1 - \nu) E / ((1 + \nu)(1 - 2\nu))$  is the uniaxial strain modulus, and  $G$  is the shear modulus. The effective interfacial toughness depends on geometric parameters as well as interface and bulk material properties. This dependency can be expressed in terms of nondimensional parameters. The parameters that define the edge-cracked bimaterial strip problem include interfacial properties  $\sigma^*$ ,  $\Gamma$ ,  $\lambda$ , and  $\tau^*$ , elastic layer properties  $\rho$ ,  $E$ ,  $\nu$ , elastic layer height  $h$ , and the Rayleigh mass damping coefficient  $m_d$  (units of  $\mu\text{s}^{-1}$ ). The nondimensional parameters can be expressed in terms of  $\Gamma$ ,  $\sigma^*$ , and  $\rho$  (other choices are possible; this is simply a convenient choice). With this choice, length ( $\mu\text{m}$ )  $\sim \Gamma/\sigma^*$ , force ( $\mu\text{N}$ )  $\sim \Gamma^2/\sigma^*$ , and time ( $\mu\text{s}$ )  $\sim (\Gamma/\sigma^*)/(E/\rho)^{1/2}$ . Accordingly, the effective toughness can be expressed as

$$\Gamma_e/\Gamma = f\left(\frac{\sigma_{xy}^c}{\sigma_{yy}^c}, \frac{\tau^*}{\sigma^*}, \frac{\sigma^*}{E}, \frac{h}{(2\Gamma/\sigma^*)}, \nu, \lambda, \frac{2m_d\Gamma}{\sigma^*(E/\rho)^{1/2}}\right) \quad (3)$$

The present study is focused on the effect of varying the relative amount of applied shear-to-normal loading  $\sigma_{xy}^c/\sigma_{yy}^c$ . In these illustrative calculations, the linear elastic strip is defined by  $h = 1 \mu\text{m}$ ,  $E = 1 \text{ GPa}$ ,  $\nu = 1/3$ ,  $\rho = 1 \text{ g/cm}^3$ , and  $m_d < 5000 \mu\text{s}^{-1}$  while the Ad/AF model parameters are  $\Gamma = 0.05 \text{ J/m}^2$ ,  $\sigma^* = 50 \text{ MPa}$ ,  $\tau^*/\sigma^* = 0.5$ , and  $\lambda = 0.05$ . Note that the choice of  $\tau^*/\sigma^* = 0.5$  is arbitrary; a known relationship between these parameters is not implied.

Fig. 3 illustrates the nature of the interfacial tractions that are generated when the Ad/AF surface interaction model is used. These results are for  $\sigma_{xy}^c/\sigma_{yy}^c = 0.25$ , and for this case the calculated value of  $\sigma_{yy}^c$  is  $13.67 \text{ MPa}$ . The calculated interfacial normal traction  $T_n$  and tangential traction  $T_t$  that occur just prior to crack propagation are plotted. Here the crack tip is defined as located at the point where  $T_n = \sigma^*$ . The adhesive zone length  $L_a$  is defined as the region where  $T_n$  decreases with increasing normal interfacial separation  $\delta_n$  (i.e.,  $\delta_n > \lambda\delta_n^c$  in Fig. 1a), and the slip zone length  $L_s$  is defined as the region where  $T_t = \tau^*$  (Fig. 3). Note that  $T_t$  vanishes within the adhesive zone since  $\delta_n > \lambda\delta_n^c$  in this region. As shown in the figure, the normalized length of the fully developed adhesive zone,  $L_a/h$ , equals  $0.0250$ , while that of the fully developed slip zone,  $L_s/h$ , equals  $0.0275$ . In this calculation, the adhesive zone is  $\sim 10$  elements long ( $\Delta = 0.0025 \mu\text{m}$ ). This calculation was rerun with a refined mesh with  $\Delta = 0.00125 \mu\text{m}$  to assess solution convergence with element size. There was only a  $0.4\%$  change in the calculated value of  $\sigma_{yy}^c$ . Another calculation showed that reducing the amount of damping by decreasing the Rayleigh mass damping coefficient from  $m_d = 5000 \mu\text{s}^{-1}$  to  $200 \mu\text{s}^{-1}$  had no effect on the calculated  $\sigma_{yy}^c$ .

The calculated critical value of the normal stress at crack propagation  $\sigma_{yy}^c$  depends on the relative level of the applied shear

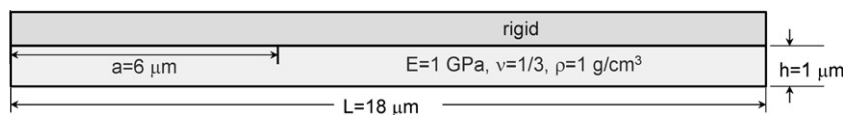


Fig. 2. A long, edge-cracked bimaterial strip with uniform edge-normal and edge-tangential displacements applied to the upper rigid material while the bottom edge of the lower elastic material is fixed.

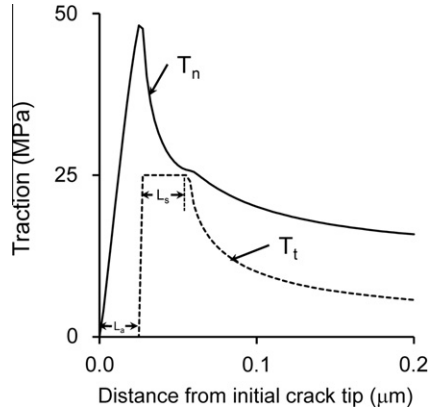


Fig. 3. Calculated interfacial normal traction  $T_n$  and tangential traction  $T_t$  just prior to crack propagation.

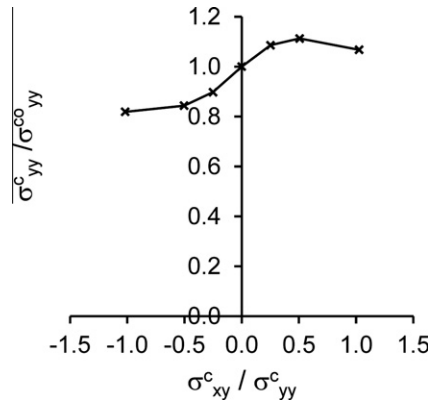


Fig. 4. Critical normal stress at crack propagation vs the ratio of shear-to-normal applied ligament stress.

$\sigma^c_{xy}/\sigma^c_{yy}$  (Fig. 4). Here  $\sigma^c_{yy}$  is normalized by its value when  $\sigma^c_{xy}/\sigma^c_{yy} = 0$ ,  $\sigma^c_{yy}/\sigma^c_{0yy}$ . The value of  $\sigma^c_{yy}/\sigma^c_{0yy}$  varies from 0.82 to 1.07 as  $\sigma^c_{xy}/\sigma^c_{yy}$  varies from  $-1$  to  $1$  and as such indicates an asymmetry in the dependence. As an aside, the linear elastic fracture mechanics solution for the same problem as analyzed here (but without adhesion or atomistic friction) also displays an asymmetric dependence on the sign of  $\sigma^c_{xy}/\sigma^c_{yy}$  (Hutchinson and Suo, 1992). For example, at a distance  $\Delta = 0.0025 \mu\text{m}$  behind the crack tip (i.e., one element length), the value of  $\delta_n$  for  $\sigma^c_{xy}/\sigma^c_{yy} = -0.25$  is 1.45 times larger than that for  $\sigma^c_{xy}/\sigma^c_{yy} = 0.25$ .

Equation (2) can be used in conjunction with the calculated critical stresses  $\sigma^c_{xy}$  and  $\sigma^c_{yy}$  to determine how  $\Gamma_e/\Gamma$  varies with the relative level of the applied shear  $\sigma^c_{xy}/\sigma^c_{yy}$ . In order to provide a formal connection to the crack-tip mode mixity as defined in linear elastic fracture mechanics solutions for an interface crack, an applied mode mixity  $\psi_a$  is defined as

$$\psi_a \equiv \tan^{-1} \left( 2\sigma^c_{xy}/\sigma^c_{yy} \right) \quad (4)$$

The crack tip mode mixity a distance  $l_0$  in front of a long interfacial crack in an elastic, semi-infinite bimaterial strip held between rigid grips (i.e., the same problem as analyzed here, but without adhesion and atomistic friction) can be expressed as (Hutchinson and Suo, 1992)

$$\psi_{r=l_0} = \gamma + \omega + \varepsilon \ln(l_0/h) \quad (5)$$

If the upper material is rigid and the lower elastic material has a Poisson's ratio of  $1/3$ , then  $\varepsilon = -0.081$ ,  $\omega = -17^\circ$  and  $\gamma = \psi_a$  (as defined by Eq. (4)) for plane strain. The reference length is arbitrary,

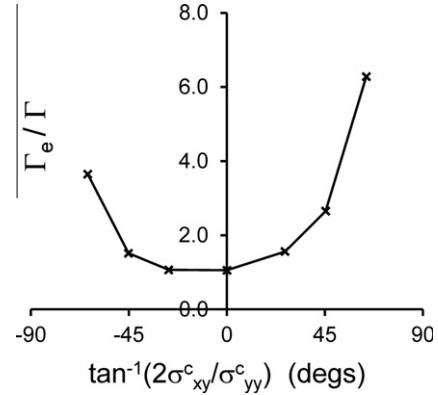


Fig. 5. Effective toughness  $\Gamma_e$  vs. the applied mode mixity.

but is often chosen as some fixed material length scale. If  $l_0/h = 0.01$ , then  $\omega + \varepsilon \ln(l_0/h) = 4.5^\circ$ . It is important to note, however, that the linear elastic fracture mechanics solution is applicable only when the lengths of the adhesive zone  $L_a$  and the slip zone  $L_s$  are both small relative to the region dominated by the stress singularity (i.e., when there is “small-scale yielding”). Fig. 5 shows that the effective toughness (normalized by the work of adhesion  $\Gamma$ ) does display a strong dependence on applied mode mixity. The calculated  $\Gamma_e/\Gamma$  has a minimum value of 1.06 when  $\psi_a = 0^\circ$  (note,  $\Gamma_e/\Gamma = 1.07$  when  $\psi_a = -27^\circ$ ). There is a clear asymmetry with respect to  $\psi_a$ . When  $\psi_a = -64^\circ$ ,  $\Gamma_e/\Gamma = 3.65$ . When  $\psi_a = 64^\circ$ ,  $\Gamma_e/\Gamma = 6.28$ . Interestingly, the calculated dependence of  $\Gamma_e$  on  $\psi_a$  is qualitatively similar to that which has been observed experimentally. For example, the toughness of an epoxy/glass interface shows a strong dependence on crack-tip mode mixity (Liechti and Chai, 1992). In this case the mode-dependent energy dissipation was attributed to epoxy yielding. An epoxy/self-assembled monolayer-coated sapphire interface also displays a strong dependence on crack-tip mode mixity, although in this case the energy dissipation was attributed to a mode-dependent intrinsic toughness (Mello and Liechti, 2006).

Energy dissipation due to frictional slip is presumably the primary source of the dependence of  $\Gamma_e$  on  $\psi_a$ . Fig. 6 shows that the length of the slip zone displays a similar dependence on  $\psi_a$ . The slip zone vanishes when  $\psi_a = 0^\circ$ , but becomes relatively large compared to layer height  $h$  as  $|\psi_a|$  increases. When  $\psi_a = -64^\circ$ ,  $L_s/h = 0.28$ . When  $\psi_a = 64^\circ$ ,  $L_s/h = 0.37$ . As an aside, the length of the adhesive zone  $L_a$  is relatively insensitive to the value of  $\psi_a$  ( $0.025 \leq L_a/h \leq 0.035$ ). The magnitude of the frictional energy dissipation/unit area is equal to  $\tau^* \delta_s$ , where  $\delta_s$  is the maximum frictional slip (found at the tip of the adhesive zone where the normal interfacial stress  $\sigma = \sigma^*$ ). Fig. 7 plots the normalized

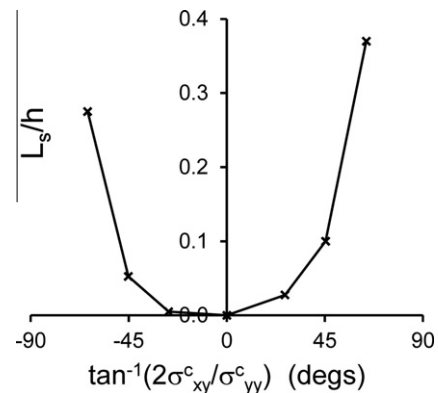


Fig. 6. Length of the fully developed slip zone  $L_s$  vs. the applied mode mixity.



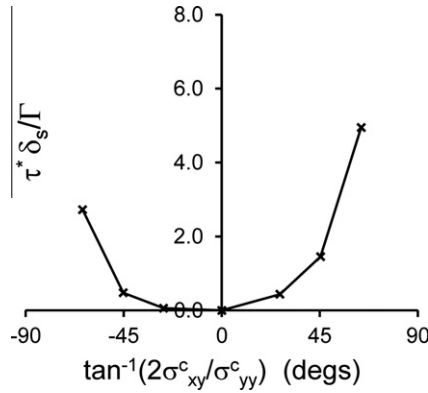


Fig. 7. Energy dissipated by frictional slip,  $\tau^* \delta_s$ , vs. the applied mode mixity.

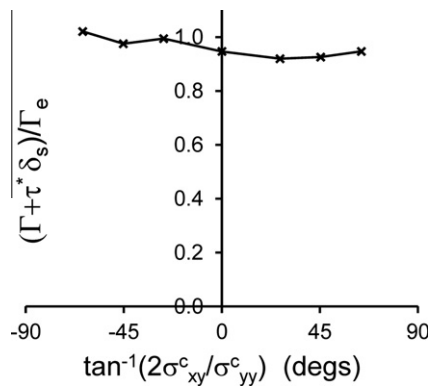


Fig. 8. The fraction of the effective toughness that is attributable to the sum of the energy dissipated by normal interfacial separation (work of adhesion) and frictional slip.

frictional dissipation energy/unit area vs.  $\psi_a$ . A comparison of Figs. 5 and 7 plainly indicates that energy dissipation associated with frictional slip is the primary source of the dependence of  $\Gamma_e$  on  $\psi_a$ . This is more clearly shown in Fig. 8. The fraction of the effective toughness that is attributable to the energy dissipated by normal interfacial separation (work of adhesion) and friction slip,  $(\Gamma + \tau^* \delta_s) / \Gamma_e$ , is plotted as a function of  $\psi_a$ . The calculated values  $(\Gamma + \tau^* \delta_s) / \Gamma_e$  are close to one, with a maximum deviation of 8%. This suggests that the energy dissipation associated with stress waves (vibrations) generated by the abrupt release of the frictional stress as the adhesive zone forms is relatively small. It is worth noting that amount of frictional slip that can occur in these calculations can be relatively large compared to the element size. For instance,  $\delta_s / \Delta \sim 4$  when  $\psi_a = 64^\circ$ .

#### 4. Nano-embossing

Adhesion and atomistic friction are expected to impact both embossing and release steps in a nanofabrication process when feature size is on the order of 10's to 100's of nanometers. Typically a relatively stiff mold (e.g., silicon, quartz) is used to imprint or hot emboss a polymer (e.g., photoresist etch barrier). Since the mold must be released from the hardened polymer without damaging the molded pattern, some means to weaken the adhesion between the mold and polymer is normally employed. Consequently, nano-fabrication simulations should use a polymer/solid surface interaction model like the Ad/AF model since it is applicable to solids that interact via relatively weak, van der Waals forces. A series of illustrative simulations was performed to explore the impact of using the Ad/AF model in simulations of a nano-embossing process

(results for release after nano-embossing can be found elsewhere (Reedy and Cox, 2013)). To avoid geometric complexity, a 2-D, plane strain problem with a pattern composed of identical, parallel channels (or conversely teeth) was analyzed. The polymer material is heated well above its glass transition temperature and is in a rubbery state while it is embossed. Hence, the polymer is modeled as a compressible, Mooney–Rivlin rubber (Aklonis and MacKnight, 1983; Scherzinger and Hammerand, 2007) with a nominal, small strain Young's modulus of one MPa and a Poisson's ratio of 0.499 (defined by Mooney–Rivlin model parameters  $C_{10} = 0.1333$  MPa and  $C_{01} = 0.0333$  MPa). A unit cell analysis is applicable to the parallel-channel geometry and Fig. 9 shows the unit cell geometry of the embossing problem that was analyzed. Since the mold material is much stiffer than the rubbery polymer, it can be considered rigid. For this reason only elements that define the mold contour (interface) are included in the mesh. The mold cavity is nominally 100 nm wide by 50 nm high with a  $\sim 12^\circ$  wall-taper and 5-nm radii at wall transition points. The bottom edge of the polymer layer is fixed to model attachment to a relatively rigid substrate.

Calculations were performed for three cases: (a) simple contact ( $\Gamma = 0.0$  J/m<sup>2</sup> and  $\tau^* = 0.0$  MPa), (b) adhesion only ( $\Gamma = 0.05$  J/m<sup>2</sup> and  $\tau^* = 0.0$  MPa), and (c) adhesion and atomistic friction ( $\Gamma = 0.05$  J/m<sup>2</sup> and  $\tau^* = 10.0$  MPa). The range of the adhesive force in these calculations is  $\delta_n^c = 1$  nm. Fig. 10a–c shows the calculated deformed geometry at first contact of the polymer with the top surface of the mold. The downward mold displacement at first contact of the polymer with the top surface of the mold,  $U_{contact}$ , the displacement to fill the mold,  $U_{fill}$ , and the applied compression to fill the mold  $C_{fill}$  (defined as the applied compressive load at the time when the mold cavity is completely filled/base area) is displayed on each of the figures. The addition of adhesion causes the polymer to jump into contact once it is within range of the adhesive force and helps pull the polymer into the corner. This yields a 30% lower calculated value of  $C_{fill}$  (compare cases a and b). The further addition of atomistic friction results in an even greater effect on the polymer deformation (compare cases b and

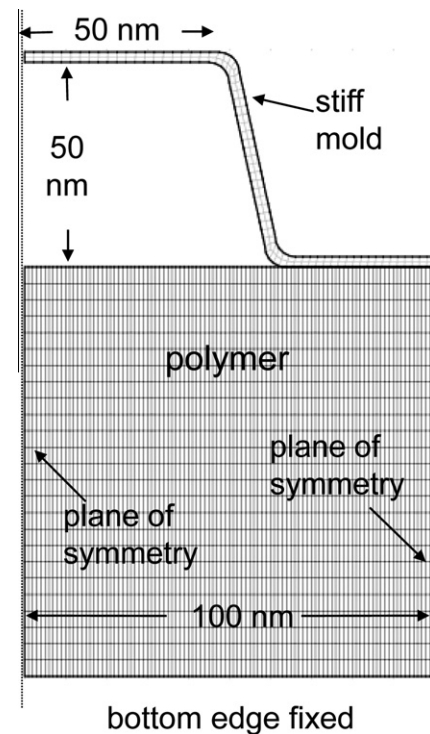
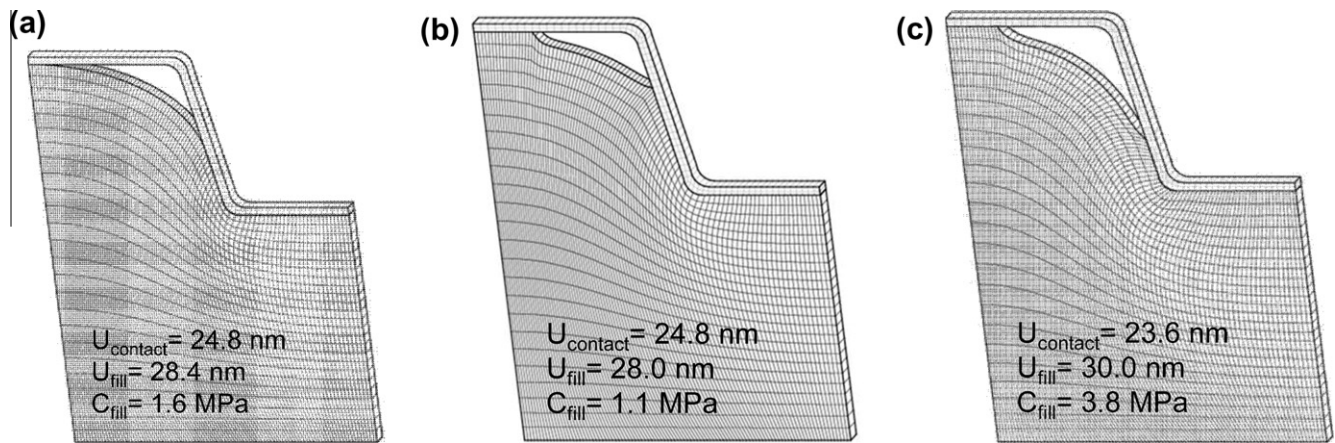
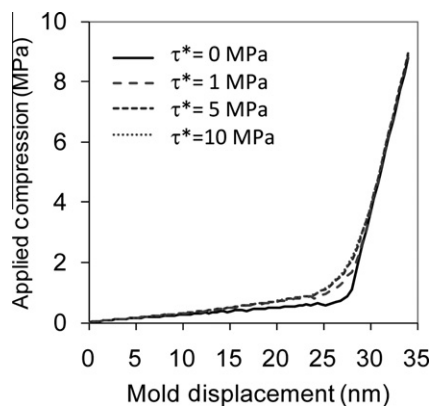


Fig. 9. Unit cell geometry used in the embossing simulations.



**Fig. 10.** The calculated deformed geometry at first contact of the polymer with the top surface of the mold for (a) no adhesion or atomistic friction, (b) adhesion but no atomistic friction, and (c) adhesion and atomistic friction. Values of  $U_{\text{contact}}$ , the displacement at first contact of the polymer with the top surface of the mold,  $U_{\text{fill}}$ , the displacement to fill the mold, and  $C_{\text{fill}}$ , the applied compression to fill the mold are displayed on the plots.



**Fig. 11.** Applied compression vs. mold displacement for different levels of atomistic friction.

c). While adhesion pulls the polymer towards the mold, atomistic friction retards fill by preventing slip. The further addition of atomistic friction increases the calculated  $C_{\text{fill}}$  from 1.1 to 3.8 MPa, an increase of 350%. Note that sidewall adhesion and friction also affect the maximum height of the polymer at the center of the mold prior to the polymer's first contact with the top surface of the mold. Relative to the case of no friction or atomistic friction (Fig. 10a), the polymer is pulled higher up the sidewall when there is adhesion but no atomistic friction (Fig. 10b). On the other hand, the polymer is not pulled as far up the sidewall when there is both adhesion and atomistic friction (Fig. 10c). Since the polymer is nearly incompressible, the sidewall contact area varies inversely with the polymer's height at the center of the mold. As a consequence the mold displacement needed to induce polymer contact at the top of the mold,  $U_{\text{contact}}$ , is least when there is both adhesion and friction (Fig. 10).

The sensitivity of the embossing simulations to the values of the parameters  $\Gamma$  and  $\tau^*$  that govern the strength of polymer/mold interactions was also investigated. The adhesion only analysis was rerun but with  $\Gamma$  reduced from 0.05 to 0.005 J/m<sup>2</sup> (i.e.,  $\sigma^* = 10$  instead of 100 MPa, while maintaining  $\delta_c = 1$  nm). There was no discernible difference generated by reducing  $\Gamma$ . The rubbery polymer is so compliant and the polymer stresses are so low prior to the time when the mold is completely filled that even an interfacial strength of 10 MPa will cause the polymer to jump into contact. The adhesion with atomistic friction simulations were also rerun with varying values of  $\tau^*$ . Fig. 11 shows that the applied compression to fill the mold is altered even when  $\tau^* = 1$  MPa.

Results for  $\tau^* = 5$  and 10 MPa are essentially identical indicating that the polymer is fully stuck to the mold surface (i.e., no slip) and further increase in  $\tau^*$  will not affect the calculated response. Note that the applied compressive load increases rapidly once the mold is completely filled since the deformation is then determined by the polymer's much higher bulk modulus ( $U_{\text{fill}} = 28.0, 29.2, 30.0$  and  $30.0$  nm for  $\tau^* = 0, 1, 5$ , and  $10$  MPa, respectively).

The illustrative results presented here clearly show that adhesion and atomistic friction can have a significant effect on a nano-embossing process. The polymer deformation pattern is altered and a significantly higher load is required to push the last portion of polymer material into the corner of the mold. These results suggest that atomistic friction may make it increasingly difficult to push a rubbery polymer into the top corner of a feature as feature height increases. These results also suggest that high accuracy measurements of  $\tau^*$  may not be necessary. Even a small value of  $\tau^*$  sticks a rubbery polymer to the mold wall, and increasing that value has no effect.

## 5. Summary

A novel adhesion/atomistic friction (Ad/AF) surface interaction model for solid materials interacting through van der Waals dispersive forces has been formulated and implemented in an explicit dynamics finite element code. Illustrative interfacial fracture and nano-embossing simulations were presented. The classic problem of bimaterial strip with a long edge crack held between rigid grips was analyzed. The Ad/AF surface interaction model generates a strongly mode-dependent effective interfacial toughness (i.e., depends on the relative level of the applied shear). This dependence is a direct outcome of Ad/AF model. The nano-embossing simulations indicate that even low levels of adhesion and atomistic friction can have a significant effect on nanofabrication processes. As the mold is pushed into a rubbery polymer during embossing, adhesion pulls the polymer towards the mold while atomistic friction retards fill by preventing slip. The two primary parameters that define the Ad/AF model ( $\Gamma$  and  $\tau^*$ ) can, at least in principle, be measured directly using AFM friction force microscopy techniques.

## Acknowledgments

This work was supported by the Laboratory Directed Research and Development Program at Sandia National Laboratories. Sandia National Laboratories is a multi-program laboratory managed and

operated by Sandia Corporation, a wholly owned subsidiary of Lockheed Martin Corporation, for the U.S. Department of Energy's National Nuclear Security Administration under contract DE-AC04-94AL85000.

## References

- Aklonis, J.J., MacKnight, W.J., 1983. Introduction to Polymer Viscoelasticity. John Wiley and Sons.
- Barrenblatt, G.I., 1962. The mathematical theory of equilibrium of cracks in brittle fracture. *Adv. Appl. Mech.* 7, 55–129.
- Burns, A.R., Houston, J.E., Carpick, R.W., Michalske, T.A., 1999. Molecular level friction as revealed with a novel scanning probe. *Langmuir* 15, 2922–2930.
- Carpick, R.W., Flater, E.E., Sridharan, K., Ogletree, D.F., Salmeron, M., 2004. Atomic-scale friction and its connection to fracture mechanics. *JOM* 56, 48–52.
- Corwin, A.D., de Boer, M.P., 2004. Effect of adhesion on dynamic and static friction in surface micromachining. *Appl. Phys. Lett.* 84 (13), 2451–2453.
- Costner, E.A., Lin, M.W., Jen, W.L., Willson, C.G., 2009. Nanoimprint lithography materials development for semiconductor device fabrication. *Annu. Rev. Mater. Res.* 39, 155–180.
- Crosby, A.J., Hageman, M., Duncan, A., 2005. Controlling polymer adhesion with “pancakes”. *Langmuir* 21, 11738–11743.
- DelRio, F.W., de Boer, M.P., Knapp, J.A., Reedy Jr., E.D., Clews, P.J., Dunn, M.L., 2005. The role of van der Waals forces in adhesion of micromachined surfaces. *Nat. Mater.* 4, 629–634.
- Derjaguin, B.V., Muller, V.M., Toporov, Y.P., 1975. Effect of contact deformations on the adhesion of particles. *J. Colloid Interface Sci.* 53, 314–326.
- Gates, B.D., Xu, Q.B., Stewart, M., Ryan, D., Willson, C.G., Whitesides, G.M., 2005. New approaches to nanofabrication: molding, printing, and other techniques. *Chem. Rev.* 105 (4), 1171–1196.
- Glassmaker, N.J., Jagota, A., Hui, C.Y., Kim, J., 2004. Design of biomimetic fibrillar interfaces: 1. Making contact. *J. R. Soc. Interface* 1 (1), 23–33.
- Hui, C.Y., Jagota, A., Lin, Y.Y., Kramer, E.J., 2002. Constraints on microcontact printing imposed by stamp deformation. *Langmuir* 18 (4), 1394–1407.
- Hutchinson, J.W., Suo, Z., 1992. Mixed mode cracking in layered materials. In: Hutchinson, J.W., Wu, T.Y. (Eds.), *Advances in Applied Mechanics*. Academic Press, vol. 29, pp. 63–191.
- Johnson, K.L., Kendall, K., Roberts, A.D., 1971. Surface energy and the contact of elastic solids. *Proc. Royal Soc. London. Ser. A* 324, 301–313.
- Kendall, K., 1994. Adhesion – molecules and mechanics. *Science* 263 (5154), 1720–1725.
- Kent, M.S., Yim, H., Matheson, A., Cogdill, C., Nelson, G., Reedy Jr., E.D., 2001. Use of self-assembled monolayers at variable coverage to control interface bonding in a model study of interfacial fracture: pure shear loading. *J. Adhes.* 75 (3), 267–298.
- Liechti, K.M., Chai, Y.S., 1992. Asymmetric shielding in interfacial fracture under in-plane shear. *J. Appl. Mech.* 59, 295–304.
- Maboudian, R., Ashurst, W.R., Carraro, C., 2002. Tribological challenges in micromechanical systems. *Tribol. Lett.* 12 (2), 95–100.
- Mello, A.W., Liechti, K.M., 2006. The effect of self-assembled monolayers on interfacial fracture. *J. Appl. Mech.* 73 (5), 860–870.
- Needleman, A., 1987. A continuum model for void nucleation by inclusion debonding. *J. Appl. Mech.* 54 (3), 525–531.
- Reedy Jr., E.D., 2006. Thin-coating contact mechanics with adhesion. *J. Mater. Res.* 21 (10), 2660–2668.
- Reedy Jr., E.D., 2007. Contact mechanics for coated spheres that includes the transition from weak to strong adhesion. *J. Mater. Res.* 22 (9), 2617–2622.
- Reedy Jr., E.D., Cox, J.V., in press. Hierarchical analysis of the release step in a nanofabrication process using an adhesion/atomistic friction surface interaction model. *J. Eng. Mater. Technol.*
- Reedy Jr., E.D., Starr, M.J., Jones, R.E., Flater, E.E., Carpick, R.W., 2005. Contact modeling of sam-coated polysilicon asperities. In: 28th Annual Meeting of the Adhesion Society. Mobile, AL.
- Scherzinger, W.M., Hammerand, D.C., 2007. Constitutive Models in LAME, SAND2007-5873, Sandia National Laboratories.
- Thomas, J.D., 2011. Sierra/SolidMechanics 4.22 User's Guide, SAND2011-7597. SIERRA Solid Mechanics Team Albuquerque, Sandia National Laboratories.
- Tvergaard, V., Hutchinson, J.W., 1992. The relation between crack growth resistance and fracture process parameters in elastic–plastic solids. *J. Mech. Phys. Solids* 40 (6), 1377–1397.
- Yang, Y., Ruths, M., 2009. Friction of polyaromatic thiol monolayers in adhesive and nonadhesive contacts. *Langmuir* 25, 12151–12159.
- Newby, B.M.Z., Chaudhury, M.K., 1998. Friction in adhesion. *Langmuir* 14 (17), 4865–4872.